Intensity-based Registration versus Feature-based Registration for Neurointerventions

Robert A. McLaughlin[a*]   John Hipwell[b†]   Graeme P. Penney[b]   Kawal Rhode[b]   Albert Chung[a]

J. Alison Noble[a]

David J. Hawkes[b]

[a] Medical Vision Laboratory, Dept of Engineering Science, University of Oxford, England,
[b] CISG, Division of Radiological Sciences, Guy's Hospital, King's College London, London, England.

Abstract. Registration of 2D-3D data sets can provide an important tool to help visualisation during minimal invasive neurointerventions. We have quantitatively compared two approaches to this registration problem: an intensity-based algorithm and a feature-based algorithm. The intensity-based algorithm was found to be more accurate, having an average RMS error of 1.2 mm, compared to 2.3 mm for the feature-based algorithm. However, the feature-based algorithm proved to be more reliable over a wide range of starting conditions.

1 Introduction

Registration of 2D-3D data is important in minimal invasive neurointerventions, such as the embolisation of brain aneurysms. During such an operation, a neuroradiologist guides a catheter through blood vessels, while viewing its progress on real-time 2D X-ray images. Because these X-ray images are only a 2D projection, they do not give depth information. This can make accurate navigation difficult, because of the hidden 3D structure of the vessels.

A pre-operative CTA or MRA scan can be used to generate a 3D model of the blood vessels in the patient's brain. Given a robust and accurate 2D-3D registration algorithm, it would be possible to correlate the position of the catheter viewed on the 2D X-ray image with the 3D model. This would enable the neuroradiologist to view the position of the catheter, superimposed upon a computer-generated 3D visualisation of the brain.

Using an in-vitro silicon aneurysm phantom (middle cerebral artery bifurcation aneurysm), we evaluate the accuracy and robustness of two different types of registration algorithm for such a task: an intensity-based algorithm [1] and a feature-based algorithm [2].

2 Method

Both of the following methods register a segmented 3D model of blood vessels from MRA or CTA with a digital subtraction angiography (DSA) image.

2.1 Intensity-based Registration

The intensity-based registration algorithm [1] iteratively optimises the six rigid-body parameters describing the orientation of the 3D dataset, by generating digitally reconstructed radiographs (DRRs) and comparing these with the DSA image using a gradient difference similarity measure [3]. Some minor modifications to the algorithm of [1] were required to adapt it to work with segmented 3D data and DSA images, rather than unsegmented CT data and fluoroscopy images.

To reduce processing time a multi-resolution strategy was adopted whereby the DRRs and DSA images were sub-sampled by a factor of four. These dimensions were subsequently doubled until the optimisation of the parameters was completed with both images at their full resolutions. In addition, two manually drawn regions of interest were used, the first, and smaller of the two, enabling an initial approximate registration to be obtained, whilst the second, larger region of interest promoted its refinement by incorporating more peripheral structures.

2.2 Feature-based Registration

The feature-based registration algorithm presented in [2] first generates a 'skeleton' of the blood vessels present in the DSA image, reducing the thickness of each to a single pixel. Blood vessels in the 3D model are also

---

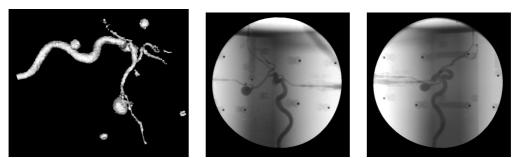*ram@robots.ox.ac.uk
†john.hipwell@kcl.ac.uk

Figure 1. Visualisation of 3D phantom data and two DSA images.

'skeletonised', by extracting the medial axis of each vessel. The algorithm then selects a sub-sample of points on the 3D skeleton model. For each 3D point, the closest corresponding point in the 'skeletonised' DSA image is found using a territory-based correspondence search as described in [2]. Using these pairs of points and the method outlined in [4], the algorithm iteratively finds the optimal rotation and translation of the 3-D model to achieve a registration. The registration was performed in two stages. An initial result was computed using the larger region-of-interest that was previously utilised by the intensity-based algorithm. This was then refined using the entire image. This use of a region of interest is an extension upon the algorithm presented in [2].

2.3 Calculation of "Gold-Standard" Registration

We obtained both CTA and phase-contrast MRA scans of an in-vitro silicon aneurysm phantom. Date expired whole blood was introduced into the phantom using a Pulsatile Blood Pump 1405 (Harward Apparatus) operating at 200ml/min. A 3D visualisation of the segmented MRA data set is shown in Figure 1. We also obtained two sets of pre- and post-contrast X-ray images of the phantom at different orientations of the X-ray gantry.

The CTA scan was obtained using a GE Medical Systems Hispeed Advantage with voxel size $0.48 \times 0.48 \times 1.0$ mm and image dimensions $512 \times 512 \times 175$ voxels. Blood was segmented using a combination of thresholding and mathematical morphological operations. The phase-contrast MRA scan was obtained using a GE Medical Systems Signa Echospeed 1.5T with voxel size $0.86 \times 0.86 \times 1.0$ mm and image dimensions $256 \times 256 \times 124$ voxels. It was segmented as described in [5]. The X-ray images were acquired using a GE Medical Systems Advantx DX, and digitised from the PAL composite video signal at an image resolution of 512×512 pixels. During the injection of a contrast agent, three seconds of images were acquired at twenty five frames per second. These were used to generate two images: a maximal image where the images were combined so that a maximum level of contrast is seen in each pixel, and a single-frame image, where an image half way through the run was chosen. A pre-contrast mask image was then subtracted from both images to generate the DSA images. Typical DSA images produced are shown in Figure 1.

A distortion-correction phantom and software were used to correct for pincushion distortion in the fluoroscopy images [3]. The "gold standard" registration was found using an acrylic calibration phantom containing 14 embedded ball bearings, and also eight fiducial markers positioned around the phantom itself. Several of the fiducials can be seen in Figure 1. The calibration phantom enabled the intrinsic perspective transformation parameters to be calculated whilst the positions of the fiducial markers specify the extrinsic rigid-body parameters.

2.4 Experiments for Accuracy and Robustness

The segmented CTA data was registered with both maximal and single-frame DSA images. Starting positions for the registrations were chosen by perturbing the gold standard values by set amounts. This methodology was adopted from [3]. Four experiments were performed, with the amount of perturbation increased each time, as shown in Table 1. For each experiment, different combinations of the four perturbations resulted in sixteen different starting positions. Note that there were no in-plane translations (δX or δY), as these can be accurately calculated by selecting a single corresponding point in both the DSA image and the DRR simulated from the CTA data.

The same experiments were then repeated to register the MRA volume with each DSA image.

To measure the accuracy of the registrations, we use the reprojection distance as defined by Masutani et al. [6]. A number of points identifying particular features on the segmented 3D model were chosen, along with the corre-

Experiment #	δZ	$\delta\theta_x$	$\delta\theta_y$	$\delta\theta_z$
1	±25 mm	$\pm4°$	$\pm4°$	$\pm4°$
2	±50 mm	$\pm8°$	$\pm8°$	$\pm8°$
3	±75 mm	$\pm12°$	$\pm12°$	$\pm12°$
4	±100 mm	$\pm16°$	$\pm16°$	$\pm16°$

Table 1. Perturbations of the starting positions from the gold standard for four of the six rigid-body parameters.
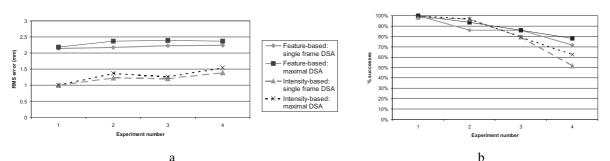

a   b

Figure 2. (a) Registration accuracy. (b) Registration reliability

sponding points in the DSA image. Using the rotation and translation matrix resulting from each registration, we re-computed the position of the 3D points. We then calculated the minimum distance (in mm) from each point to the ray passing from the X-ray source to the corresponding DSA image point. This gives a measurement of the accuracy of the registration when projecting from 3D to 2D. A discussion of the measurement can be found in [3]. Finally, we computed the average RMS error of all such points for each experiment. If the average RMS error for a particular registration was less than 4 mm, the registration was judged to have succeeded.

3 Results

Figure 2a plots registration accuracy for each algorithm, using both the maximal DSA image and the single-frame DSA image. Figure 2b plots the percentage of successful registrations. Only successful registrations were used in computing the accuracies shown. Results of typical registrations are displayed in Figure 3.

4 Discussion

As can be seen from Figure 2, the intensity-based algorithm was found to have better accuracy than the feature-based algorithm, while the feature-based algorithm converged to the correct solution more reliably, over a wider range of starting conditions. Both algorithms achieved high reliability in Experiments one and two where the starting positions were perturbed from the gold-standard value by only small amounts (see Table 1). Reliability of the intensity-based algorithm degraded in Experiments three and four, where perturbations from the gold standard were increased. Under these conditions, performance of the feature-based algorithm was more reliable.

Recall that the feature-based algorithm registers a skeleton of the 3D model with a skeleton of the DSA image. It is thus sensitive to inaccuracies in the position of the skeletonised points. This accounts for its lower accuracy when
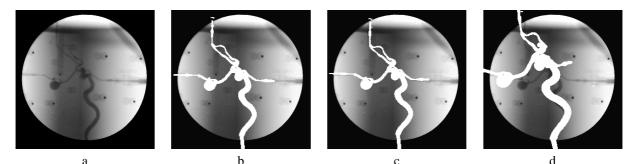

a   b   c   d

Figure 3. Results of registration. Registered 3-D vessels are overlaid in white. (a) Original DSA image. (b) Result of intensity-based registration. (c) Result of feature-based registration. (d) Typical failed registration.

compared to the intensity-based algorithm, which registers the intensity values of individual pixels. However, the greater reliability of the feature-based algorithm shown in Figure 2b suggest that points on the skeletonised vessels can be robustly extracted under rotations and translations of the volume. In contrast, the intensity values of individual pixels can vary greatly under these conditions. This accounts for the lower reliability of the intensity-based algorithm when the starting positions vary from the gold-standard by medium amounts.

The intensity-based algorithm requires at least partial superposition of vessels in the DRR and DSA image at all times throughout the iterative process for a successful registration to be achieved. Because of this, the algorithm was found to be sensitive to in-plane rotations as these can have a dramatic effect upon the superposition of vessels in the two images. If vessel overlap is lost at any time, the correct registration will not be found and the algorithm will converge to a local minimum.

The feature-based algorithm was found to be sensitive to the quality of both the 2D and 3D skeletonisation algorithms used. A poor skeletonisation of the data was seen to lead to poor registration.

The computation time of the algorithms has important ramifications for the clinical suitability of both approaches to registration. We noted that the feature-based algorithm was far less computationally intensive than the intensity-based algorithm, resulting in a much faster registration. This is because the feature-based algorithm operates on a small number of skeletonised points, rather than the exhaustive pixel-based approach of the intensity-based algorithm. In future work, we will seek to quantify these differences.

5   Conclusion

We have compared an intensity-based and a feature-based registration algorithm on DSA images of a neurovascular phantom. The DSA images were registered to both CTA and MRA data. The intensity-based registration algorithm was found to give more accurate registrations, with a typical RMS reprojection error of approximately 1.2 mm. The feature-based algorithm was found to have a typical RMS reprojection error of approximately 2.3 mm.

The feature-based algorithm was found to converge to the correct solution with greater reliability. This demonstrates that we could robustly find correspondences in the skeletonised features. In contrast, the intensity-based algorithm failed once vessel overlap was lost.

Our results suggest the development of a hybrid algorithm, using the feature-based algorithm for a reliable initial registration, then refining this result with the more accurate intensity-based registration. Future work will be to develop such an extended algorithm, and further quantify the strengths and weaknesses of the two approaches. Validation of both approaches upon clinical data is currently being done.

Acknowledgements

References

1. G. P. Penney, J. Weese & J. A. L. et al. "A comparison of similarity measures for use in 2-D-3-D medical image registration." *IEEE Trans. Medical Imaging* **17(4)**, pp. 586–595, 1998.
2. Y. Kita, D. L. Wilson & J. A. Noble. "Real-time registration of 3D cerebral vessels to X-ray angiograms." In *MICCAI'98*, pp. 1125–1133. 1998.
3. G. P. Penney. *Registration of Tomographic Images to X-ray Projections for Use in Image Guided Interventions*. Phd thesis, University College London, CISG, Division of Radiological Sciences, Guy's Hospital, King's College London, London SE1 9RT England, 2000.
4. J. J. Heuring & D. W. Murray. "Visual head tracking and slaving for visual telepresence." In *Proc. of IEEE Int. Conf. on Robotics and Automation*, pp. 2908–2914. 1996.
5. A. C. S. Chung & J. A. Noble. "Statistical 3D vessel segmentation using a Rician distribution." In *MICCAI'99*, pp. 82–89. 1999.
6. Y. Masutani, T. Dohi & F. Y. et al. "Interactive virtualized display system for intravascular neurosurgery." In *CVRMed-MRCAS'97*, pp. 427–435. 1997.